Elevated temperature response of RC beams strengthened with NSM FRP bars bonded with cementitious grout

Citation for published version:
Del Prete, I, Bilotta, A, Bisby, L & Nigro, E 2020, 'Elevated temperature response of RC beams strengthened with NSM FRP bars bonded with cementitious grout', *Composite Structures*. https://doi.org/10.1016/j.compstruct.2020.113182

Digital Object Identifier (DOI):
10.1016/j.compstruct.2020.113182

Published In:
Composite Structures

Elevated temperature response of RC beams strengthened with NSM FRP bars bonded with cementitious grout

Iolanda Del Prete[1], Antonio Bilotta[2], Luke Bisby[3], Emidio Nigro[2]

ABSTRACT

This paper presents the results of 12 tests on small-scale reinforced concrete beams strengthened in flexure with a single NSM carbon FRP bar. The used FRP bar is a novel commercial bar with high values of glass transition T_g and decomposition T_d temperature to improve the performance of the strengthening system at elevated temperature. The FRP is bonded using a cementitious grout rather than an epoxy adhesive. Flexural tests were performed at both ambient and elevated temperatures on both un-strengthened and strengthened beams. Tests at elevated temperature were performed using propane-fired radiant panels, rather than a fire testing furnace, in two heating configurations (localised heating near midspan only and global heating over the entire bonded length of the FRP systems).
This paper also shows the results of Dynamic Mechanic Analysis (DMA), Thermogravimetric Analysis (TGA) and Differential Scanning Calorimetry (DSC) tests conducted on the CFRP. The results of thermal conductivity tests of CFRP and cementitious grout, and tests conducted to define the mechanical properties of concrete, steel bars, cementitious grout and CFRP bar are discussed herein.
The flexural tests demonstrated the grout-bonded NSM CFRP strengthening system's ability to maintain structural effectiveness at temperatures up to about 600°C with adequate anchorage. However, similar tests with an epoxy adhesive are needed before the novel system can be confidently stated as being vastly superior to epoxy-adhered NSM systems.

1. INTRODUCTION

The aging of the built heritage and infrastructures throughout the civil and industrialized world, as well as their deterioration due to environmental effects, and/or changing in service demand, lead to increasing interest in novel techniques aimed to design, maintain and rehabilitate concrete structures.
Among the available strengthening techniques for improving the performance of concrete structures, the strengthening with Fibre Reinforced Polymers (FRP) gained huge and fast popularity during the last twenty-five years in the field of civil engineering.
In the field of external strengthening of RC members the strengthening technique that experienced a widespread in the recent years is the Near Surface Mounted (NSM) strengthening system, whereby the FRP is placed into the groove, cut into the surface of structural members and bonded through an adhesive (epoxy resin or cement mortar).
The available literature about the behaviour of NSM FRP strengthened RC members is still limited, if compared to that available for the EBR strengthening technique.

[1] BuroHappold Engineering, 17 Newman Street W1T 1PD, London - UK
[2] Department of Structures for Engineering and Architecture, University of Naples, via Claudio 21 80125, Naples - Italy
[3] Institute for Infrastructure & Environment, School of Engineering, University of Edinburgh, Mayfield Road EH9 3JL, Scotland UK

Even worse is the knowledge about NSM with cementitious adhesives in not ordinary condition (fire). For this reason, very limited indications are available in the current codes for designing and predicting the capacity of the NSM strengthened members.
The available literature has demonstrated that NSM bonded with an epoxy adhesive exhibits superior bond behaviour compared with externally-bonded FRP reinforcement (EBR) (El-Hacha et al [1], Foret et al [2], Bilotta et al [3]). NSM is also less prone to damage, since the FRP is embedded in a groove and inside the adhesive. Despite this, the effectiveness of epoxy adhesives is severely reduced at elevated temperatures. Ambient temperature cure epoxy adhesives are characterized by relatively low glass transition temperatures (T_g), however higher T_g values can be achieved for pultruded FRP which is manufactured at elevated temperature. In NSM applications, using an elevated T_g FRP product bonded with a cementitious grout may result in superior mechanical performance in fire, since cementitious adhesives may perform better than epoxies, whilst also protecting (both mechanically and thermally) the FRP, possibly without the need to apply costly and unattractive supplemental insulation materials to the exterior of the FRP strengthening system (Yu et al [4]). Even though epoxy resins are usually used as bonding agents, there have been several recent studies on the behaviour of cementitious paste or mortar bonded NSM FRP systems (Yu et al [4], Petra et al [5], Burke et al [6], Palmieri et al [7]).
The available studies regarding the fire performance of EBR FRP strengthened RC members highlighted the need to protect the members using passive fire protection systems. These researches were aimed to evaluate the minimum requirements to obtain satisfactory performances in fire (Blontrock et al [8], Bisby et al [9], Williams et al [10], Palmieri et al [11], [12], Firmo et al [13]).
Palmieri et al ([14], [15]) tested RC beams strengthened with several NSM FRP configurations, insulated and not insulated, to evaluate the fire performance. Epoxy and cementitious grouts were used on different beams to study the influence of the adhesive on the behaviour of NSM FRP system at both ambient and elevated temperatures. Despite the high service load of the strengthened beams, and the partial failure of the fire protection on some beams, all the beams were able to sustain the applied load without failure for the 2 h of ISO 834 standard fire exposure, even after the adhesive's temperature exceeded its glass transition temperature. Moreover, they found that U-shaped fire protections (extending to the sides of the beam) are more efficient than flat protections at the bottom surface of the beam only. Residual strength tests on the fire-tested beams demonstrated also that, if the insulation is able to maintain the adhesive temperature below 200 °C, the FRP is able to retain bond strength to the concrete and the beam is still able to retain part of the flexural capacity of the FRP strengthened beam at ambient condition.
Burke et al [6] presented tests of reinforced concrete slabs strengthened in flexure with a single strip of NSM FRP tape at elevated temperature (up to 200°C). Epoxy and cementitious grouts were used on different slabs. The tests' results showed that the epoxy adhesive on NSM FRP reinforcement provides higher strength in comparison to the cementitious grout at ambient temperature. These results, according to those found by Palmieri et al, were attributed to the better bond behaviour of epoxy adhesives in comparison to cementitious adhesives. However, at elevated temperature, the slabs with cementitious grout yielded higher failure time than those with epoxy adhesive. They also stated that insulated NSM FRP strengthened slabs may provide the required fire resistance for usual building applications.

Petri et al [5] tested RC slabs strengthened with NSM system through pultruded carbon fibre rods, embedded in high temperature inorganic grout, insulated with an ultra-high temperature insulation system consisting of gap filling ceramic fiber blanket and an inch thick ceramic fibre board. The tested FRP strengthening system demonstrated its capability to withstand temperatures greater than 200 ºC. They obtained a satisfactory margin of safety, for over two and a half hours of an E119 fire under the maximum permissible load with no structural deficiencies.

Kodur & Yu [16] developed a numerical model, which was able to predict the fire response of a reinforced concrete beam with NSM FRP. They observed that a concrete beam strengthened with NSM FRP reinforcement yields fire resistance (75 min) that is slightly lower than a conventional concrete beam (85 min), but higher than the resistance of a similar concrete beam strengthened with externally bonded FRP laminate (65 min). Moreover, an NSM FRP-strengthened RC beam, under fire conditions, may experience failure through rupture of the NSM reinforcement. This contrasts with the ambient temperature failure mode, which is through the crushing of concrete. The location of the FRP reinforcement has also an influence on the fire resistance of concrete beams strengthened with NSM FRP: NSM FRP at the middle of the beam soffit yields higher fire resistance (75 min) as compared to fire resistance of beams with NSM FRP located closer to the bottom corners of the beam (65 min). They also confirmed the results found by other researchers: an appropriate fire insulation can significantly enhance the fire response of RC beams strengthened with NSM FRP reinforcement, especially if U-shaped fire protections are used.

This paper presents an experimental testing program aimed at investigating the performance of a novel high temperature cementitious-bonded NSM CFRP strengthening system for concrete, which has been developed specifically to address the performance of FRP strengthening systems at elevated temperatures.

The CFRP bar used to strengthen the tested RC beams, is manufactured by *Milliken*, and it is defined *FireStrong* bar, since its elevated nominal T_g and T_d. It is a spirally wound round rod (Figure 1), which can be used to strengthen reinforced concrete structures, through the Near Surface Mounted technique: the bar is applied in a groove cut into the concrete cover of a RC member and bonded in place by filling the groove with a proper bonding agent. The manufacturer advices the use of *FireStrong* bars with a cementitious mortar, denominated *FireStrong Grout*, which is characterized by a nominal low thermal conductivity.

Figure 1. FireStrong CFRP bar

2. EXPERIMENTAL PROGRAM

The core experimental program consisted of two main parts: definition of materials' thermal and mechanical properties; flexural tests of RC beams and NSM FRP strengthened RC beams both at ambient and at elevated temperature.

2.1 Definition of Materials' Thermal Properties

Dynamic Mechanic Analysis (DMA) tests were carried out to define the T_g of the *FireStrong* CFRP bar. These tests provide the T_g based on changes of mechanical strength and energy loss during the glass transition.

Thermogravimetric Analysis (TGA) is a useful technique to define the T_d. TGA measures the amount and rate of change in the mass of a sample as a function of

temperature during a controlled temperature programme, in a controlled atmosphere.
Differential Scanning Calorimetry (DSC) evaluates the changes in material's heat capacity. Several DSC measurements were also conducted on the commercial CFR bar.
Thermal conductivity tests were carried out on the CFRP bar and *FireStrong* cementitious grout.
Typical physical properties of the cementitious grout are provided in the technical data sheet [17]. Additional information can be provided by the manufacturer upon request.

2.1.1 DMA and TGA Tests' Setup

DMA tests were carried out through a DMA analyser (Figure 2) performed according to ISO 6721-1:2011 [18]. The DMA experimental program is made of 6 tests: 3 tests in single cantilever (SC) configuration and 3 tests in three-point bending (TPB) configuration. The tested specimens in SC and TPB configurations are respectively shown in Figure 3 and Figure 4. Their dimensions are summarised in Table 1. It should be noted that the samples were extracted from the core of the CFRP bar by hand, hence the dimensions were not perfectly equal. Their respective size was measured as accurate as possible.

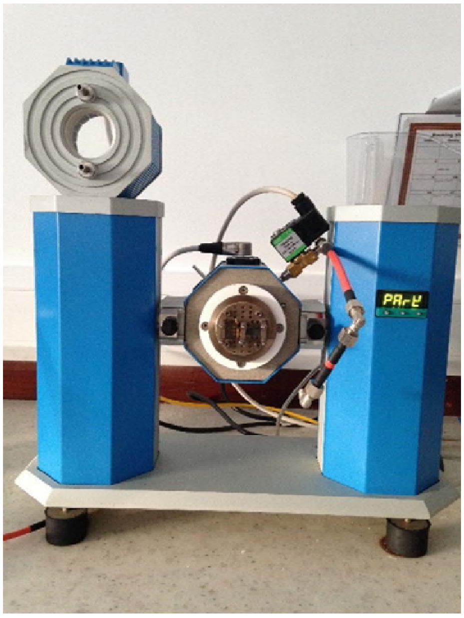

Figure 2. Dynamic mechanic analyzer in single cantilever configuration

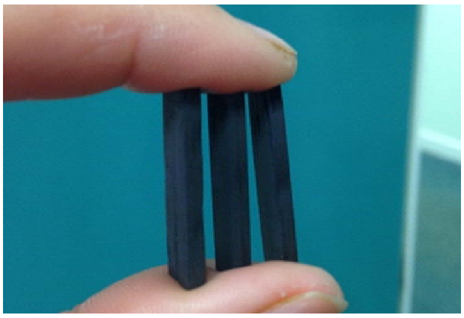

Figure 3. Specimens for DMA tests in single cantilever configuration

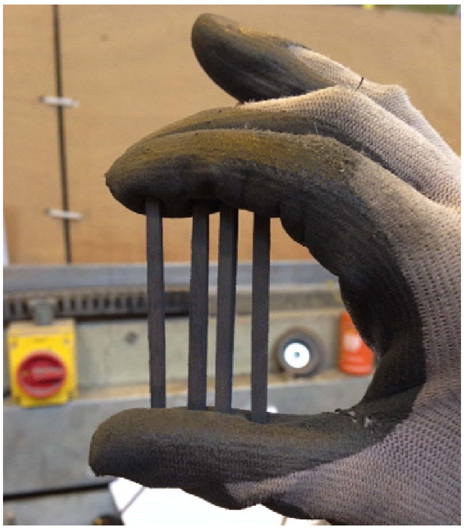

Figure 4. Specimens for DMA tests in three-point bending configuration

Table 1. DMA specimens' dimensions

Configuration	**Label**	**Dimension**		
		Length L (mm)	**Thickness t (mm)**	**Width w (mm)**
SC	CFRP-1-15	15.00	1.50	6.53
	CFRP-2-15		1.52	7.19
	CFRP-3-15		1.48	5.96
TPB	CFRP-1-40	40.00	2.53	3.07
	CFRP-2-40		2.80	3.47
	CFRP-3-40		3.23	3.47

When the analyser is in single cantilever arrangement, the specimen is firmly clamped on one end and excited on the other end. This arrangement is better than dual cantilever, where the specimen is clamped to both supports and excited at its midpoint. In the latter arrangement, specimens that expand considerably when heated may distort, falsifying the reading. The tests were conducted in single frequency (1 Hz), with a temperature rate 2°C/min and by setting a displacement amplitude equal to 0.05 mm.

When the analyser is in three-point bending arrangement, the ends are freely supported and the load is applied to the midpoint. The tests were conducted in single frequency (1 Hz), with a temperature rate 2°C/min and by setting a displacement amplitude equal to 0.05 mm.

TGA tests were carried out through a thermobalance with a horizontal arrangement, with 3 tests performed in Nitrogen (N_2) atmosphere, and 3 tests in air. The specimens were extracted by the core of the CFRP bar. They were placed in the 70 µl alumina crucibles, which were set in the sample holder (Figure 5) of the thermogravimetric analyzer (Figure 6).

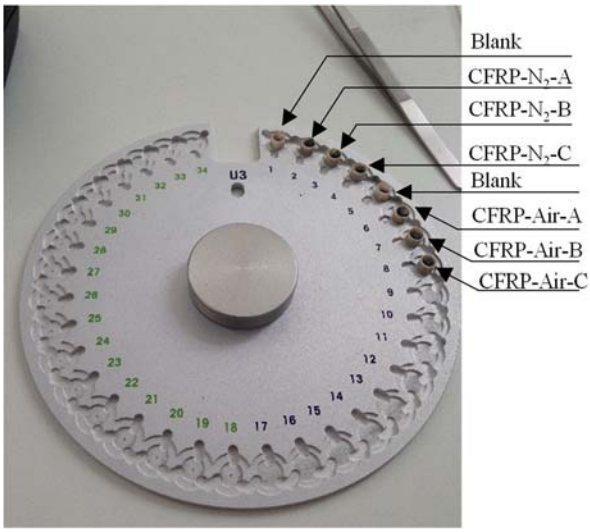

Figure 5. Specimens placed in the aluminium crucibles (70µl)

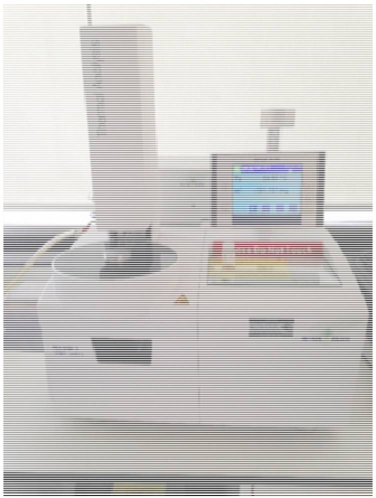

Figure 6. METTLER TOLEDO Thermogravimetric analyzer

Table 2 summarizes the specimens' initial weight and the tests' settings in terms of temperature rate and range.

Table 2. Specimens' initial weight and tests' settings TGA

Label	**Initial weight (mg)**	**Rate (°C/min)**	**Temperature range (°C)**
CFRP-N_2-A	51.6	10	25 - 800
CFRP-N_2-B	42.5		
CFRP-N_2-C	46.6		
CFRP-Air-A	47.7		
CFRP-Air-B	43.6		
CFRP-Air-C	50.2		

The Thermogravimetric Analyzer, shown in Figure 6, was used to carry out also DSC measurements, in order to define the specific heat capacity of the commercial product.

2.1.2 DMA, TGA and DSC tests' outcomes

Several standards (ISO/CD 6721 - 11:2008; DIN 65 583, 1999 [18], [19]) and apparatus manufacturers provide several techniques for determining the glass transition and decomposition temperature in practice.

Figure 7 and Figure 8 respectively show the output data of DMA and TGA analyses for one of the tested specimen, which was post-processed with the available techniques.

Figure 7 shows the normalized storage modulus E'(non-dimensional ratio between the storage modulus E', that is the real component of the stiffness of the material, and the storage modulus E' at temperature T=70°C ($E'_{70°C}$)), versus the temperature. It should be noted that the non-dimensional ratio $E'/E'_{70°C}$ enables a reasonable comparison between the results of the tests performed in SC and TPB configuration. Figure 8 shows the weight loss of one of the tested samples through the TGA measurement versus time.

As shown in Table 3 and Table 4, the observed T_g values ranged between 160°C ($T_{g,offset}$) and 220°C ($T_{g,max(tan\delta)}$), whereas T_d values ranged between 315°C ($T_{d,offset}$) and 360°C ($T_{g,midpoint}$). The variability highlights the need for clear standardization of the DMA and TGA test methods' results and the manner in which the resulting test data are processed and interpreted to get suitable ((i.e. physically representative) T_g and T_d values to be used by designers.

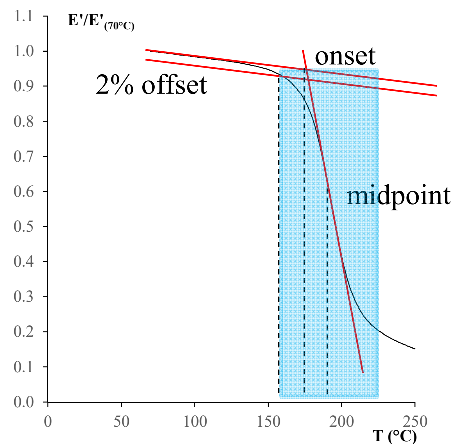

Figure 7 DMA processing methods

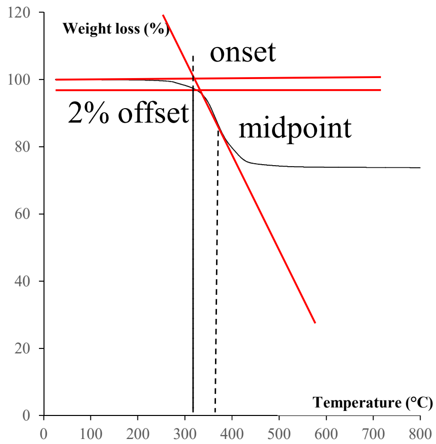

Figure 8 TGA processing methods

Table 3. **DMA outcomes**

Processing method	Analyzer arrangement	Label	T_g (°C)	μ	σ	μ	σ
Offset	SC	CFRP-1-15	160.0	161.0	3.61	170.75	10.94
		CFRP-2-15	165.0				
		CFRP-3-15	158.0				
	TPB	CFRP-1-40	180.0	180.5	0.87		
		CFRP-2-40	181.5				
		CFRP-3-40	180.0				
Onset	SC	CFRP-1-15	182.0	181.67	0.58	192.42	11.92
		CFRP-2-15	181.0				
		CFRP-3-15	182.0				
	TPB	CFRP-1-40	200.0	203.17	2.84		
		CFRP-2-40	204.0				
		CFRP-3-40	205.5				
Midpoint	SC	CFRP-1-15	192.0	194.17	2.02	205.83	12.99
		CFRP-2-15	194.5				
		CFRP-3-15	196.0				
	TPB	CFRP-1-40	214.0	217.50	3.04		
		CFRP-2-40	219.0				
		CFRP-3-40	219.5				
Peak tanδ	SC	CFRP-1-15	201.9	202.7	0.29	211.48	10.71
		CFRP-2-15	202.4				
		CFRP-3-15	201.9				
	TPB	CFRP-1-40	215.9	220.9	4.52		
		CFRP-2-40	222.0				
		CFRP-3-40	224.7				

Table 4. **TGA outcomes**

Processing method	Analyzer arrangement	Label	T_g (°C)	μ	σ	μ	σ
Offset	SC	CFRP-1-15	160.0	161.0	3.61	170.75	10.94
		CFRP-2-15	165.0				
		CFRP-3-15	158.0				
	TPB	CFRP-1-40	180.0	180.5	0.87		
		CFRP-2-40	181.5				
		CFRP-3-40	180.0				
Onset	SC	CFRP-1-15	182.0	181.67	0.58	192.42	11.92
		CFRP-2-15	181.0				
		CFRP-3-15	182.0				
	TPB	CFRP-1-40	200.0	203.17	2.84		
		CFRP-2-40	204.0				
		CFRP-3-40	205.5				
Midpoint	SC	CFRP-1-15	192.0	194.17	2.02	205.83	12.99
		CFRP-2-15	194.5				
		CFRP-3-15	196.0				
	TPB	CFRP-1-40	214.0	217.50	3.04		
		CFRP-2-40	219.0				
		CFRP-3-40	219.5				

Figure 9 shows the specific heat capacity of the CFRP bar versus temperature, calculated as a function of the heat flow (Φ) on a heated sample of known mass, measured during the DSC tests conducted on three specimens.

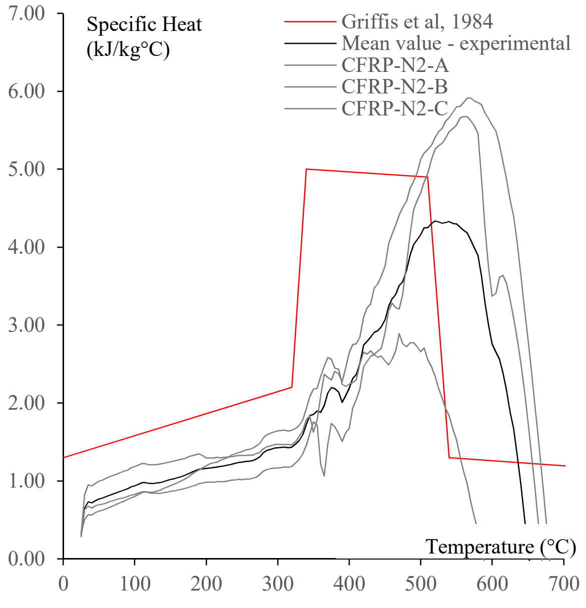

Figure 9. CFRP Specific heat capacity versus Temperature. Comparison between experimental results and the value provided in literature for a similar product

The mean value of c_p was also calculated and compared to that provided in literature for a similar carbon/epoxy product (Griffis et al [20]). According to Griffis et al, c_p linearly increased in the temperature range 20-300°C, then the slope of the curve $c_p - T$ increased significantly up to the achievement of the peak value. Referring to the mean experimental curve, after the achievement of the maximum c_p at about 545°C, the specific heat capacity suddenly decreased. Similarly, the specific heat capacity obtained by Griffis et al suddenly decreased at 500°C, but the peak value was almost constant in the temperature range 340-500°C. The perfect agreement between the experimental results and that found in literature is impossible to achieve, since the thermal properties of FRPs depend on the fibre/resin volume fraction, which can be significantly different in various products. It should be noted that after the achievement of the decomposition temperature of the CFRP bar (360 °C based on the inflection point method), the DSC results are very scattered.

The DSC measurements were not processed to determine the glass transition temperature, because DMA results were considered sufficiently reliable.

2.1.3 Thermal conductivity tests on cementitious mortar and CFRP bars

Thermal conductivity tests were performed on the cementitious grout adhesive used in the this study through the C-MATIC machine that measures the thermal conductivity of solid materials through a guarded heat flow meter. The test sample was a cylinder, 50 mm diameter and maximum 20 mm thick. This test is usually conducted by placing the sample between two plates controlled at different temperatures, resulting in a heat flow from the hotter (lower) to the colder (upper) plate. A thin heat flux transducer, attached to the lower plate, measures the amount of heat. A cylindrical guard heater, maintained at or near the mean sample temperature, surrounds the sample, in order to minimize lateral heat transfer. Built-in thermocouples measure the overall temperature difference between the two surfaces in contact with the sample.

When the sample achieves the thermal equilibrium (steady state), the Fourier heat flow equation is applied, providing the sample thermal resistance R_S that is used to calculate the thermal conductivity of the sample.

The tests yielded thermal conductivity values (essentially constant in the temperature range 50-175°C) of 0.55 W/mK; a slightly higher value (0.66 W/mK) was obtained at about 100°C. This was likely due to the evaporation of water, which led to a greater energy absorption than that needed to maintain the thermal gradient in the sample at other temperatures.

Thermal conductivity tests were also conducted on the CFRP bar by using the same machine described above. Small CFRP samples, extracted by the core of the bar, were embedded in an insulation cylinder with known thermal conductivity ($\lambda_{insulation}$). The thermal conductivity of the overall specimen (insulation plus CFRP, λ_{tot}), was measured and the CFRP thermal conductivity (λ_{CFRP}) was determined through the generally valid equation 1.

$$\lambda_{tot} = \lambda_{CFRP} \frac{V_{CFRP}}{V_{tot}} + \lambda_{insulation} \frac{V_{insulation}}{V_{tot}} \qquad 1$$

where:

$\frac{V_{CFRP}}{V_{tot}}$ is the CFRP volume fraction,

$\frac{V_{insulation}}{V_{tot}}$ is the insulation volume fraction.

The tests were conducted on six specimens, by varying the CFRP volume fraction and the fibre orientation. Three tests were performed embedding CFRP samples in the insulation cylinder with fibres parallel to the direction of the heat flux (Figure 10), in order to find the CFRP longitudinal thermal conductivity. Three tests were carried out embedding CFRP samples in the insulation cylinder with fibres perpendicular to the direction of the heat flux (Figure 10), in order to find the CFRP transverse thermal conductivity. Before testing, as recommended, the Dow Corning

340 heat sink compound was applied sparingly to both specimens' surfaces (Figure 11).

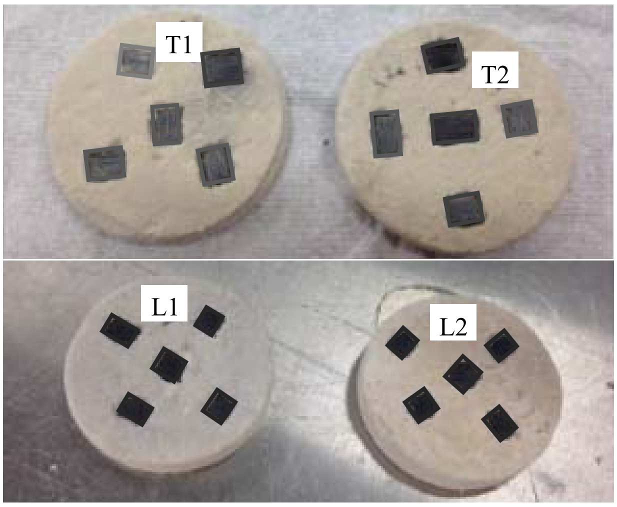

Figure 10. Specimens for thermal conductivity tests (L=longitudinal; T=transversal)

Figure 11. Specimen covered by the heat sink compound

The tests, as expected, provided a longitudinal thermal conductivity significantly higher than the transverse one (about six times). The thermal conductivities varied almost linearly in the analysed temperature range: the longitudinal thermal conductivity ranged between 5.72 W/m°C and 7.54 W/m°C in the temperature range 50°C-200°C; the transverse conductivity varied from 0.99 W/m°C to 1.29 W/m°C in the same temperature range.

2.2 Definition of Materials' Mechanical Properties

Experimental tests were carried out on at least three samples to define the relevant mechanical properties as described in the following.

<u>Concrete</u>

The mix design of the concrete batch, used to manufacture the RC beams, is summarized in Table 5.

Table 5. **Concrete mix**

COMPONENTS	QUANTITY	MOISTURE
Ordinary Portland Cement (OPC)	1002 kg	6.6
Ground Granulated Blast Furnace Slag (GGBFS)	669 kg	
Sand	1456 kg	
Aggregate 4/10 mm	3420 kg	
Additive Plastiment 180	5.04 kg	
Additive ViscoCrete 35RM	6720 ml	
Water	439 l	
W/C	0.44	

This concrete batch was tested in compression and indirect tension tests using cylindrical specimens, 200 mm high and 100 mm diameter. After the concrete was cast, the cylinders were stored in a room with controlled temperature and humidity. The tests were conducted at 28 days and at 76 days (tests days of NSM FRP strengthened RC beams at ambient temperature).
The tests at 28 days were performed through the AVERY 7104 Compression and Tension testing. The compression tests were carried out in the loading range 1000

kN, with a loading rate equal to 0.26 N/(mm^{2}s), according to ASTM C39 and UNI-EN 12390-3.
The tensile strength of the concrete was evaluated through split-cylinder tests according to IS:1999 5816-1970.
The tests at 76 days were performed through the INSTRON 600 LX, which has capacity 600 kN. The compression tests were conducted with a loading rate equal to 0.26 N/(mm^{2}s), according to ASTM C39 and UNI-EN 12390-3.
The concrete compressive and tensile strengths at 28 days were 35.6 MPa and 3.83 MPa, respectively. The concrete compressive strength at 76 days was higher than 28 days because the blended cement of this concrete batch was 60% OPC (ordinary portland cement) and 40% GGBFS (ground granulated blast furnace slag). This is a very high GGBFS content, which may retard the strength gain of the mix, leading to higher strengths at later ages.

Steel reinforcing bars (Rebars)

The rebars were tested through the INSTRON 600 LX to define the relevant mechanical properties. A unidirectional tensile load was applied with a constant speed deformation equal to 2mm/min. The free length of the tested specimens was 460 mm, the grip's length was about 55 mm, therefore the total length of the specimen was 570 mm. The specimen was painted with white random dots, in order to enable the pictures' processing through the Digital Image Correlation (DIC). This technique was very useful for measuring the displacement and the strain, as shown in the following. The strain was also calculated considering a gage length equal to 5 times the diameter, according to BS EN 10002-1:2001.
The properties are summarised in the following:

- Steel yielding strength of reinforcing bars used in tension side of the manufactured RC beams: 525 MPa;
- Steel ultimate strength of reinforcing bars used in tension side of the manufactured RC beams: 622 MPa;
- Steel yield strength of reinforcing bars used in compression side of the manufactured RC beams: 700 MPa (according to the manufacturer technical sheet).

Cementitious mortar

The grout was mixed in a high-speed mixer with the prescribed volume of potable water, until a uniform consistency was achieved, according to the Contractor Training Manual. The water/cement ratio of the mix was set equal to 0.23, according to the manufacturer technical data sheet. The tested specimen was a cylinder, 100 mm high and 50 mm diameter. The compression test was carried out through the 810 Material Testing Machine (MTS).
The cementitious mortar compressive strength at 28 days was 90 MPa. Other relevant mechanical properties are defined in the technical data sheet [17]. Additional information can be provided by the manufacturer upon request.

CFRP bars

The FireStrong CFRP bars, used to strengthen the RC beams through the NSM technique, were spirally wound round rods, 8 mm diameter. 3 Tensile tests were conducted. The free length of the tested specimens was 300 mm (~40d), according to ACI 440R.3R-04, the grip's length was 350 mm, therefore the total length of the specimens was 1000 mm. The ends of the bars were embedded in steel tubes using the two-component superfluid resin MAPEI EPOJET. The bar was loaded by gripping the steel tubes in the friction wedge of the MTS. A unidirectional tensile

load was applied with a constant speed deformation equal to 2mm/min. The specimen was painted with white random dots in order to enable the pictures' processing through the DIC. This technique provided the bar's strain, which was calculated considering a gauge length equal to 50 mm, according to ASTM D 3039/D 3039M.
The CFRP tensile strength was 1750 MPa, with a tensile elastic modulus of 136 GPa.

<u>Pull-out tests on strengthened concrete prisms</u>
Pull-out tests at ambient temperature were performed on concrete prisms strengthened with the commercial NSM-CFRP system described in this paper. The results of this experimental program are shown in Del Prete et al [21].

2.3 Flexural tests

The experimental program consisted of 12 four-point bending tests of RC beams and NSM FRP strengthened RC beams, 1450 mm long and 150 mm square in cross-section. The flexural tests were performed both at ambient and elevated temperature. The tests at elevated temperature were executed using propane-fired radiant panels to heat the beams, rather than a standard fire-testing furnace. This has the advantage of being able to provide more direct instrumentation and observation of the beams during heating, whilst still providing severe, however non-standard, heating. Two heating configurations were used: (1) localised heating near midspan only; and (2) global heating over the entire bonded length of the FRP.
The thermo-structural response was investigated under sustained loads sufficient to generate FRP strains that are typical of maximum permissible service strain conditions in the FRP (Service Load (SL) = 40 kN; High Load (HL) = 50 kN). Table 6 summarizes the flexural tests, showing the relevant test beam designations.
Ambient temperature tests were carried out after 76 days by the concrete pouring, while the elevated temperature tests were conducted on 5 months old beams, to reduce problems of concrete spalling.

Table 6. Experimental program

Beam designation	Scheme	Load
UN-S_i i=1,2	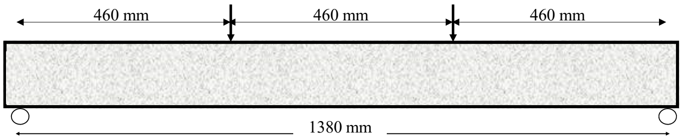	2mm/min
Note:	2 tests at ambient temperature of **UN-S**trengthened beams	
S-i i=1,2,3_cut	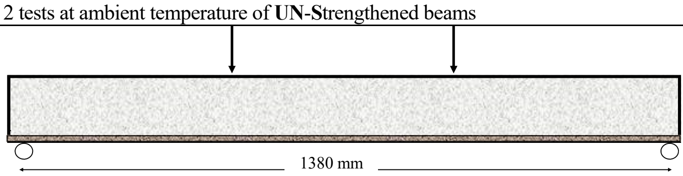	2mm/min
Note:	3 tests at ambient temperature of NSM FRP **S**trengthened beams	
UN-S_GloH_SL_1	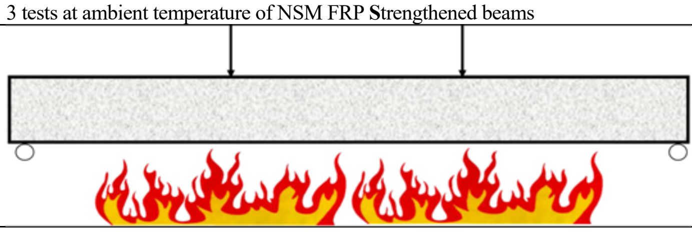	SL=40 kN
Note:	1 test of **UN-S**trengthened beam in **Glo**bal **H**eating configuration, under **S**ervice **L**oad	
S_GloH_SL_i i=1,2	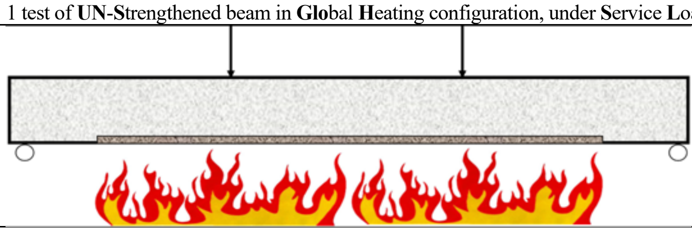	SL=40 kN
Note:	2 tests of NSM FRP **S**trengthened beams in **Glo**bal **H**eating configuration, under **S**ervice **L**oad	
S_LocH_SL_i S_LocH_HL_i i=1,2	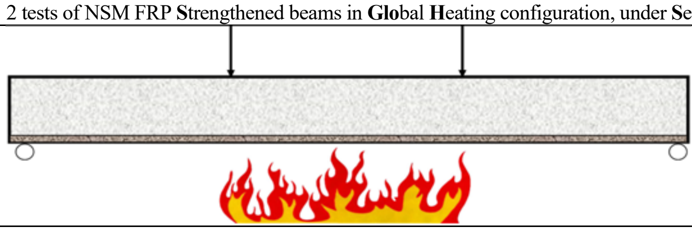	SL=40 kN HL=50 kN
Note:	- 2 tests of NSM FRP **S**trengthened beams in **Loc**alised **H**eating configuration, with **S**ervice **L**oad - 2 tests of NSM FRP **S**trengthened beams in **Loc**alised **H**eating configuration, with **H**igh **L**oad	

2.3.1 Design and Fabrication

The twelve beams had internal flexural reinforcement made of two deformed steel reinforcing bars (nominal diameter of 10 mm) on the tension side and two deformed steel reinforcing bars (nominal diameter of 6 mm) in compression (see Figure 12b).

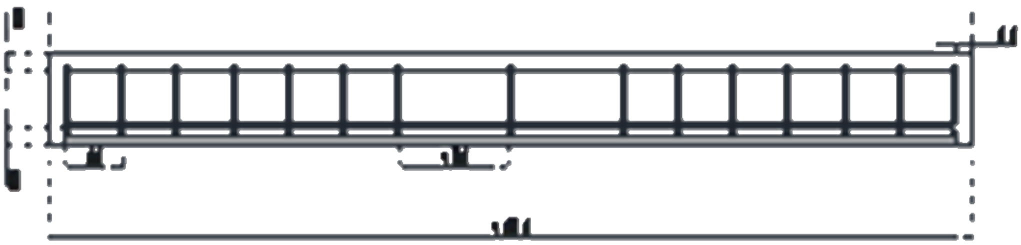

a) Longitudinal section

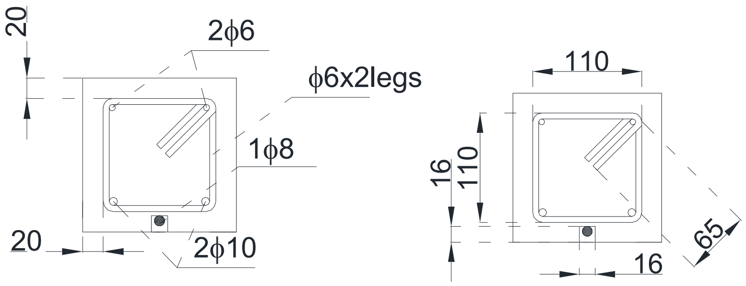

b) Cross section

Figure 12 NSM FRP strengthened RC beam

The FRP strengthening system consisted of a single CFRP bar (nominal diameter of 8 mm), grouted in place using a cementitious mortar within a groove, 16 mm square in cross-section, that was cut into the concrete cover of the beam using a ‘wall chaser’ fitted with a diamond blade. The shear reinforcement in the beams was designed to ensure that flexural failure would govern. Steel stirrups (with a nominal diameter 6 mm) were spaced at 90 mm centre-to-centre (see Figure 12a). The design of the RC beams was performed in accordance with EN1992-1 [23] and ACI 318-08 [24]; however the stirrup spacing according to EN1992-1 was adopted in the final design.

The NSM strengthening system was applied after pouring and curing of the RC beams. A wall-chasing grinder fitted with two spaced diamond cutting discs was used to cut precise vertical slots in the bottom concrete cover of the beams (Figure 13a), and the remaining fin of concrete was removed with a wall-chasing break-out tool (Figure 13b). The groove was then made smooth and clean (Figure 13c-d), and the bar was placed and grouted (Figure 13e-f), with the beams in an upside-down configuration (i.e. with gravity used to ensure complete filling of the NSM grooves).

The CFRP bar was 40 mm longer than the RC specimen (1450 mm), in order to enable the measurement of the bar’s slip through a linear potentiometer, as it will be described in the following section. Since in the real buildings the effective bonding length is usually lower than the beam length, one test at ambient temperature was conducted on a specimen (labelled S3_cut, see Table 6), with NSM bonding length equal to 1350 mm instead of 1450 mm. This enabled the evaluation of potential early failure, due to (i) lower bonding length and (ii) no local confinement provided by the supports.

Figure 13 Stages of the strengthening: a) cutting of parallel vertical slots; b) remaining fin removing; c-d) groove smoothing and cleaning; e) bar placement; f) bar grouting in cementitious mortar

2.3.2 Instrumentation and Test setup

Linear potentiometers were used during testing (both at ambient and elevated temperature) to measure the vertical displacement of the beams at midspan (LP100) and the slip of the NSM CFRP bar both at the left hand (LP25-LHS) and right hand (LP25-RHS) end of the beams (Figure 14a-b).

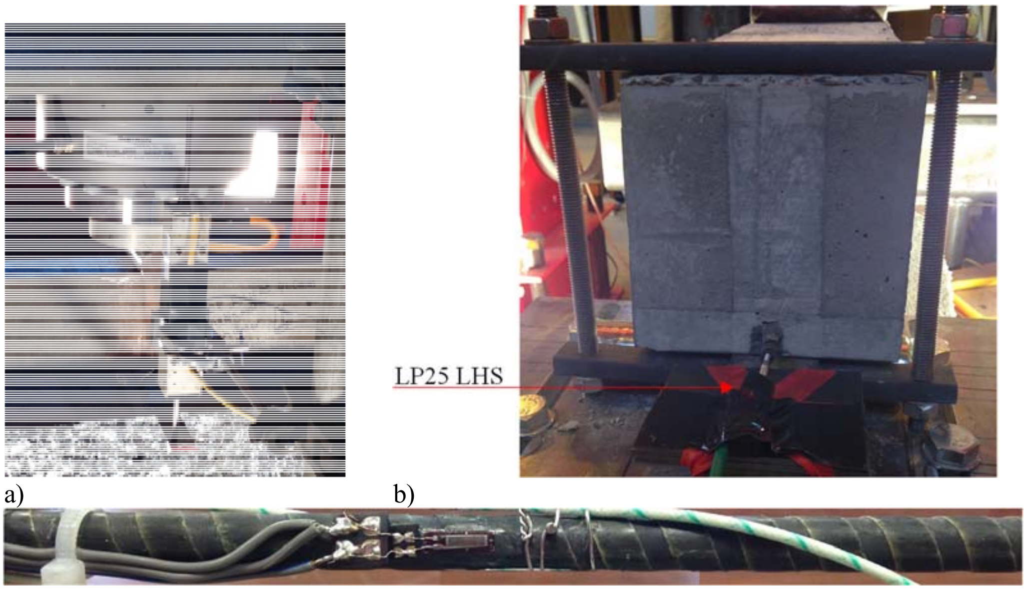

a) b)

c)

Figure 14 Flexural test setup at ambient temperature: a) main components of the setup; b) LP100; c) LP25-LHS; d) strain gauge at the mid-length of the CFRP bar

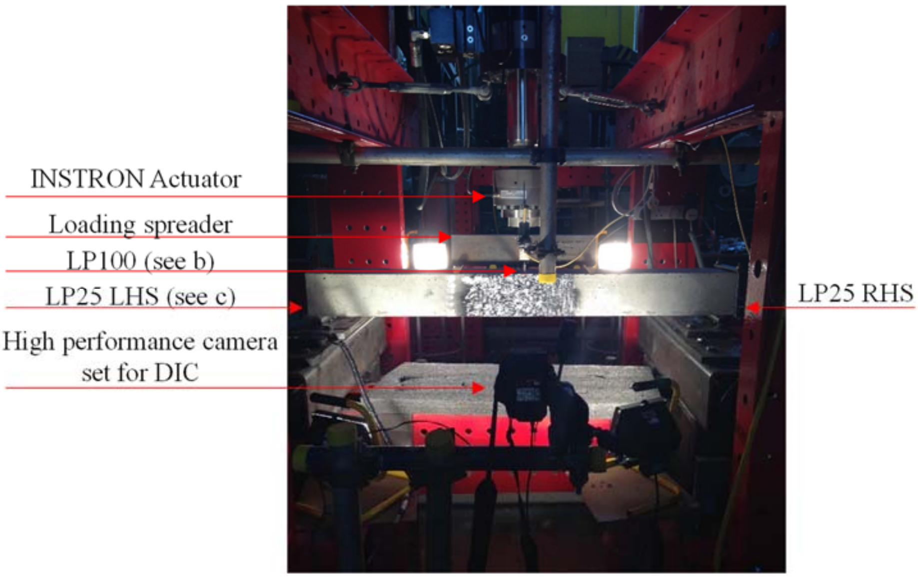

d)

A bonded foil strain gauge was also placed at the mid-length of the CFRP bar before it was installed (Figure 14c). A high-resolution digital SLR camera was set (Figure 14d) to take photos every five seconds; this enabled a DIC monitoring of the vertical deflections and flexural strains over the height of the beams. For tests at elevated temperature, multiple thermocouples (TCs) were also located within and along the beams, as shown in Figure 15.

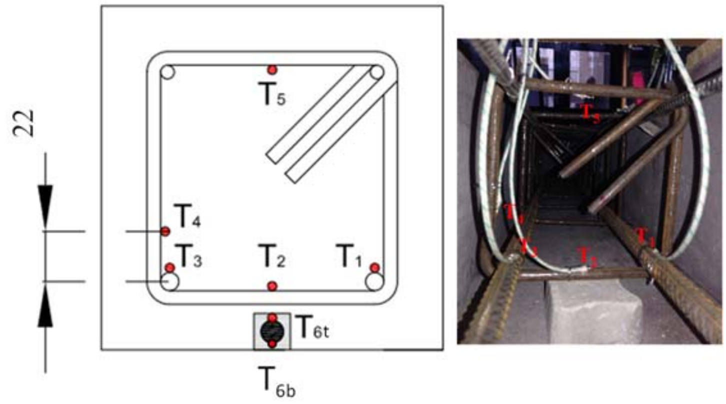

a)

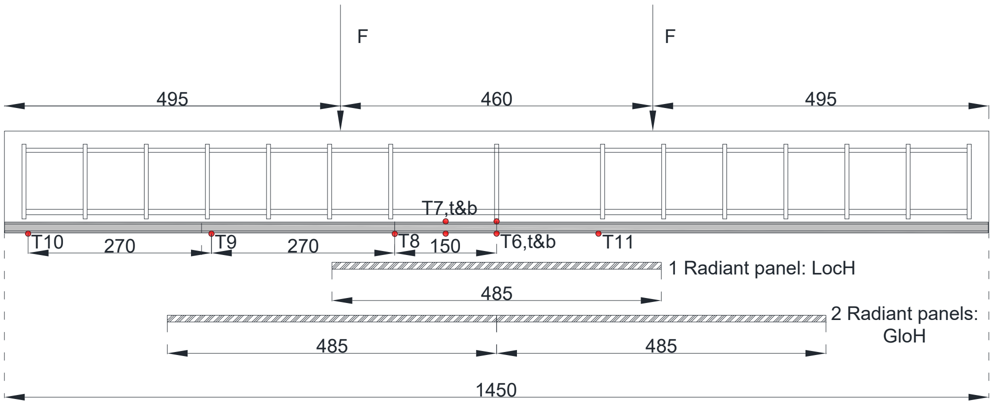

b)

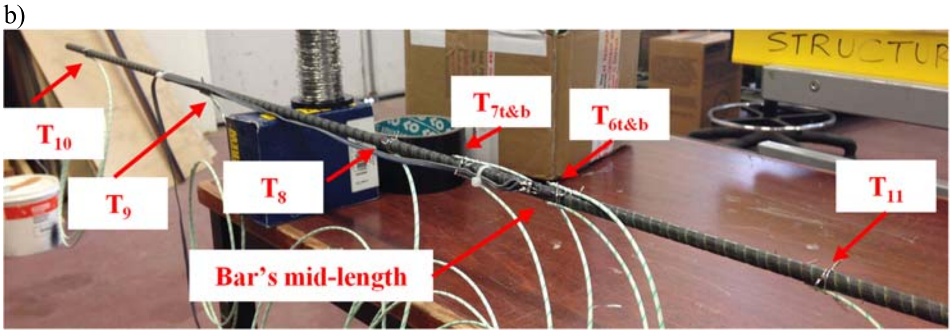

c)

Figure 15. Thermocouples' location: a) cross-section; b-c) along the CFRP bar

For the tests in local heating configuration (LocH), a propane-fired radiant heating panel was used, with plan dimensions of 485x330 mm, located at midspan 120 mm below the beams (Figure 16). The tests in global heating configuration (GloH) were carried out with two radiant heating panels, ensuring the heating over the entire bonded length of the NSM FRP strengthening system, which was 970 mm long for the beams tested in this configuration (Figure 17).
Even though the chosen heating method is a non-standard one, it can be considered highly reliable, since it provided a repeatable heat flux, as the comparison between the temperatures read by thermocouples during the tests demonstrated (Del Prete [26]).

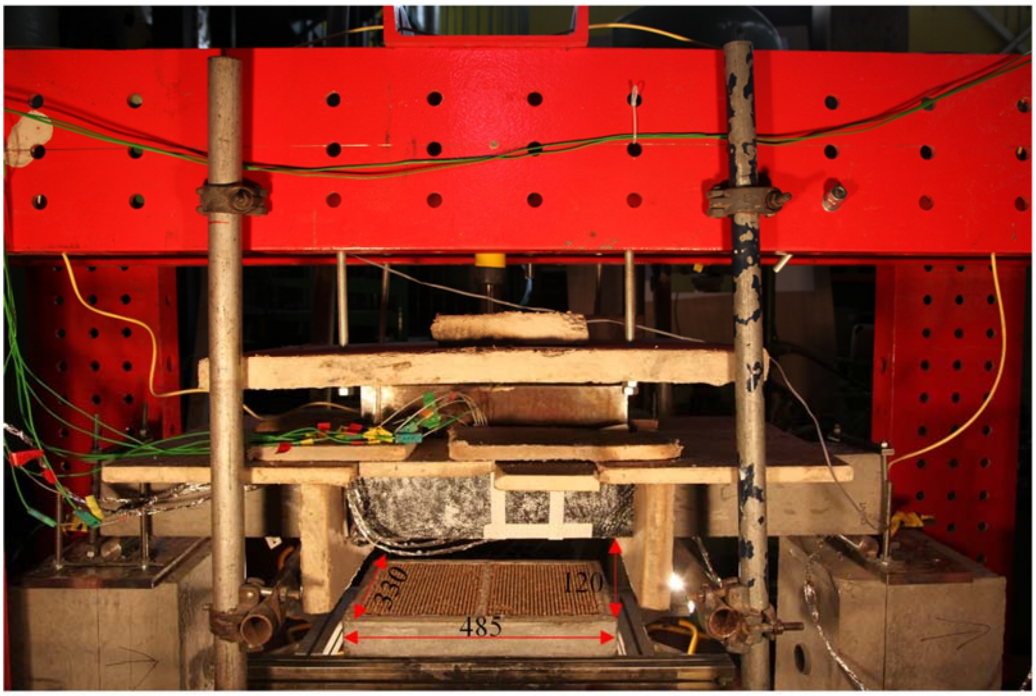

Figure 16. Radiant panel’s dimension and location in LocH configuration

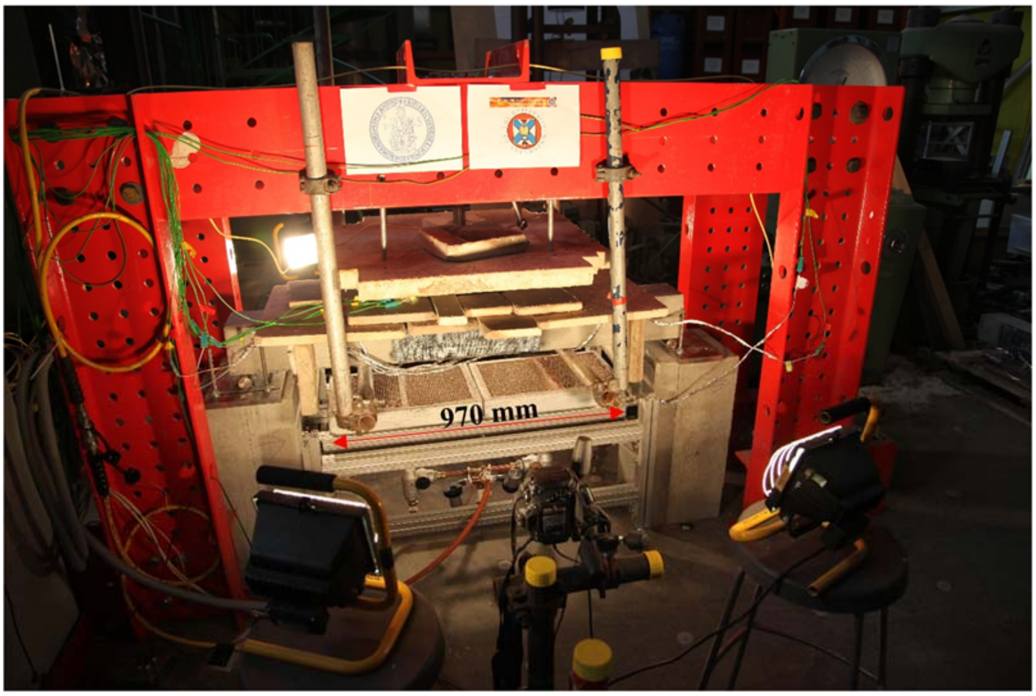

Figure 17. Radiant panels’ dimension in GloH configuration

2.3.3 Tests Results

Ambient temperature tests

The flexural tests of the strengthened beams showed that the beam cracked under a load of about 8.8 kN (Figure 18, Table 7), which is about 10% higher than the cracking load observed for un-strengthened beams. Thus, as expected the strengthening did not significantly affect the beams’ pre-cracked moment of inertia. Then, the load linearly increased until the yielding of the internal tensile reinforcement, at up to about 56 kN (36% greater than the yield load of the un-strengthened beams), which corresponded to a midspan deflection of about 9 mm. After the steel yielding, the increasing tensile loading of the CFRP bar led to the slippage between FRP bar and the cementitious bonding agent (Figure 19). The load then gradually increased up to about 59 kN (19% greater than the failure load of UN-S_1), with periodic slippage of the FRP bar resulting in a significant increase of the midspan deflection, up to about 21 mm, due to the complete debonding of the CFRP bar within the cementitious grout. After debonding of the strengthening system, which occured when the slippage of the bar was measured as about 6.7 mm (Figure 19, Table 9), the strengthened beams showed behaviour almost identical to that exhibited by the un-strengthened beams. The beam 'failure' occurred due to concrete crushing in the compression zone near the midspan (Figure 20). The strain in the CFRP bar, after concrete cracking linearly increased up to 5170 με, until the bar slippage initiated. During the gradual slippage and debonding stage, the strains in the FRP bar increased up to about 5850 με, corresponding to a slight increase in load capacity (Figure 21).

The performance of S-3_cut was slightly worse than S-1 and S-2, due to the lower bonding length (625 mm instead of 725 mm) of the bar into the groove. However, S-3_cut achieved the yielding load equal to about 54 kN (32% greater than the yielding load of the un-strengthened beams), corresponding to the midspan deflection of about 9 mm, without any damage of the strengthening system. The slippage of the bar in the groove started under a load slightly higher than the yielding load. Then, the debonding occurred leading to a significant increase of the midspan deflection up to about 24 mm.

Table 8 shows the comparison between the beams in terms of initial stiffness, calculated as ratio between the displacement and the load at cracking, and the secant stiffness, calculated as ratio between the displacement and the load at yielding. The ductility ratio of the beams has been also calculated and reported in Table 8. The ductility ratio of the strengthened beams has been calculated as ratio between the displacement achieved when the load dropped by about 19% (assumed as failure of the strengthening) and the displacement at yielding. The ductility ratio of the un-strengthened beams has been calculated as ratio between the displacement at peak load (assumed as failure load) and the displacement at yielding.

Table 7. Ambient temperature Load-displacement records

Test ID	Load at cracking (kN)	Displ. at cracking (mm)	Yielding load (kN)	Displ. at yielding (mm)	Peak load (kN)	Displ. at peak load (mm)	Failure mode
UN-S_1	8.1	0.65	40.8	7.7	50.7	34	F*
UN-S_2	7.8	0.58	40.8	7.9	45.5	34.9	F*
S-1	8.9	0.55	56.4	9.3	59.0	14.9	F/D**
S-2	8.7	0.66	56.4	9.3	59.6	17.3	F/D**
S-3_cut	8.9	0.8	54.1	9.1	56.6	17.5	F/D**

*F=Flexural; **D/F=Debonding/Flexural

Table 8. Ambient temperature records – Initial and Secant stiffness

Test ID	Initial Stiffness (kN/m)	Secant Stiffness (at yielding) (kN/m)	Ductility ratio (-)
UN-S_1	12461	5299	≥4.4
UN-S_2	13448	5165	≥4.4
S-1	16181	6065	2.3
S-2	13181	6065	2.3
S-3_cut	11125	5945	2.6

Table 9. Ambient temperature Load-slippage records

Label	Load at debonding (kN)	Slippage at debonding (mm)	Maximum CFRP strain (με)
S-1	58	6.5	5850
S-2	56	6.9	5850

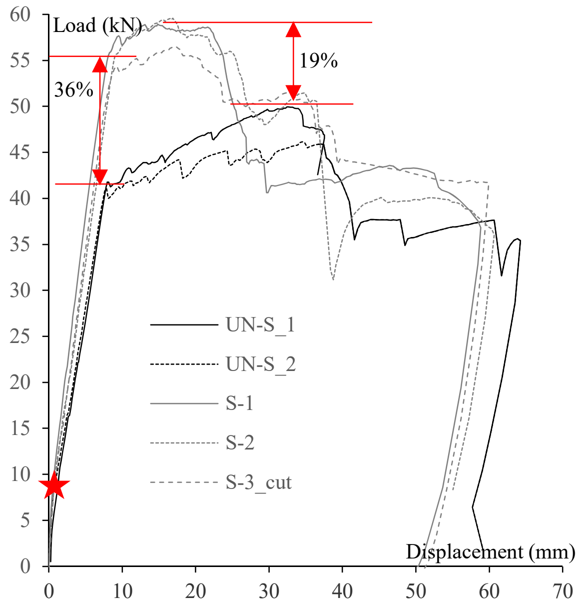

Figure 18. Load vs Displacement curves. Comparison between un-strengthened and strengthened beams.

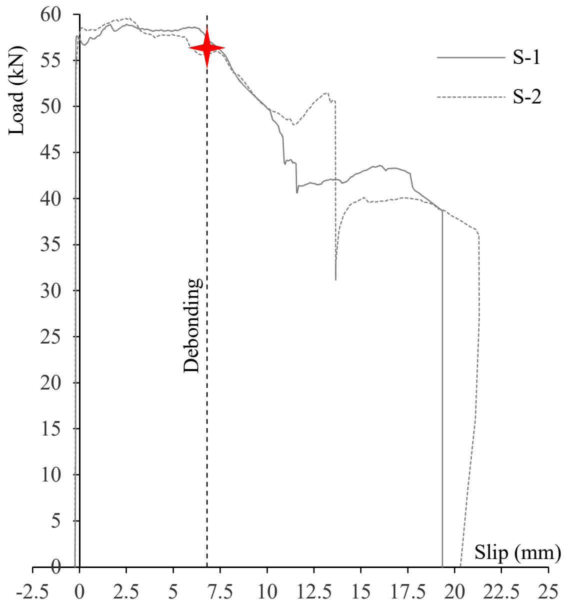

Figure 19. S-1: Load vs Slip curves. Comparison between S1 and S2

a)

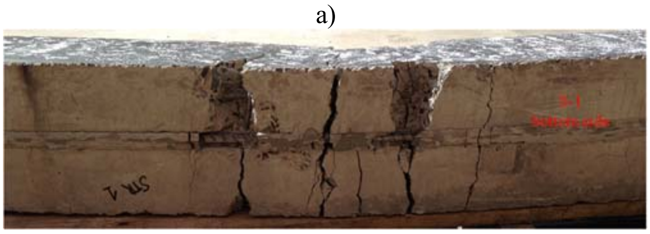

b)

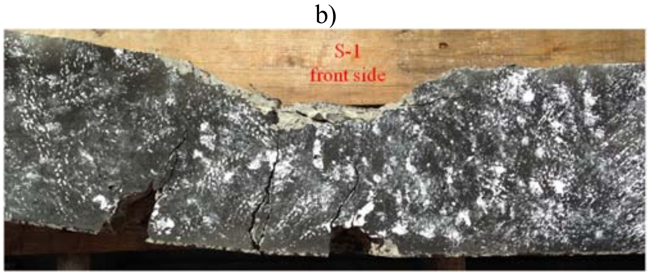

c)

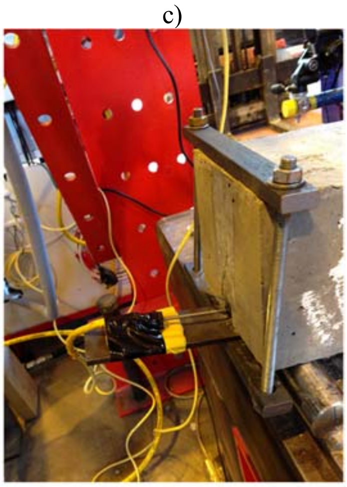

d)

Figure 20. Specimen S-1 after failure

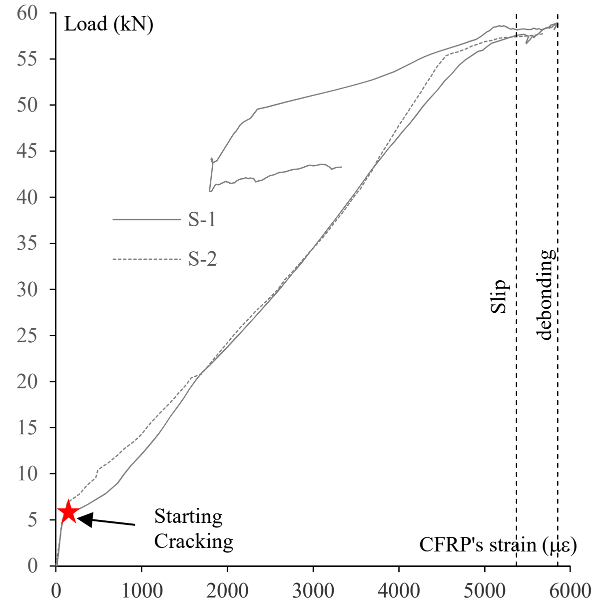

Figure 21. Load vs CFRP bar's strain. Comparison between S-1 and S-2

Elevated temperature

Figure 22 shows the temperature recorded by the thermocouples in one of the NSM FRP strengthened RC beams, tested in global heating configuration, under 40 kN sustained load (GloH-SL-1). Figure 22 shows that the temperature along the bonded length of the FRP bar (T6b – T7b – T8 – T11) is almost uniform and its maximum value, after 90 min of non-standard fire exposure, varies in the range 500-580°C. It should be noted that the temperature in the heated zone of the bar was uniform until the opening of large cracks occurred (after 50 min of fire exposure), and a maximum scatter of 80°C was recorded after 90 min of exposure. Figure 23 shows the position of the above-mentioned cracks after 90 min of heating.

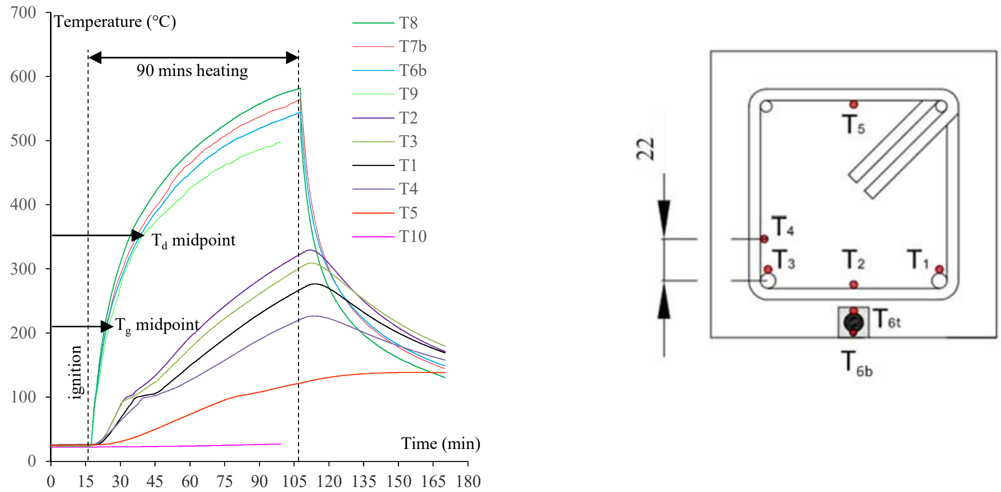

Figure 22. GloH-SL-1: Temperature versus Time curves

Figure 22 shows also that the maximum temperature in the tensile steel reinforcement (T2) was about 300°C, while it was about 65°C in the stirrup's top arm. This means that, when the strengthening system completely lost its effectiveness, due to high temperature, the un-strengthened beam was able to sustain the load, since no reduction in stiffness and resistance of steel occurred. Therefore, the beam did not fail after 90 min of heating.

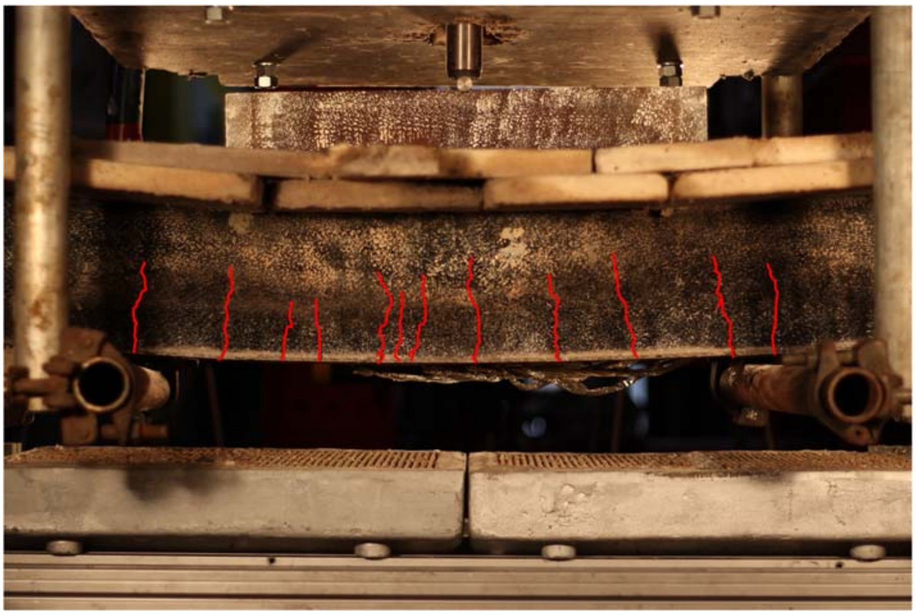

a)

b)

Figure 23. GloH-SL-1 after 90 min of heating exposure: a) front side; b) Bottom side

Figure 24 shows the temperature recorded by the thermocouples placed in one of the NSM FRP strengthened RC beams tested in local heating configuration. This figure shows that the temperature along the bonded length of the bar, after 90 min of fire exposure, varies in the range 580-630°C near the exposed midspan, while it is about 30-50 °C near the supports

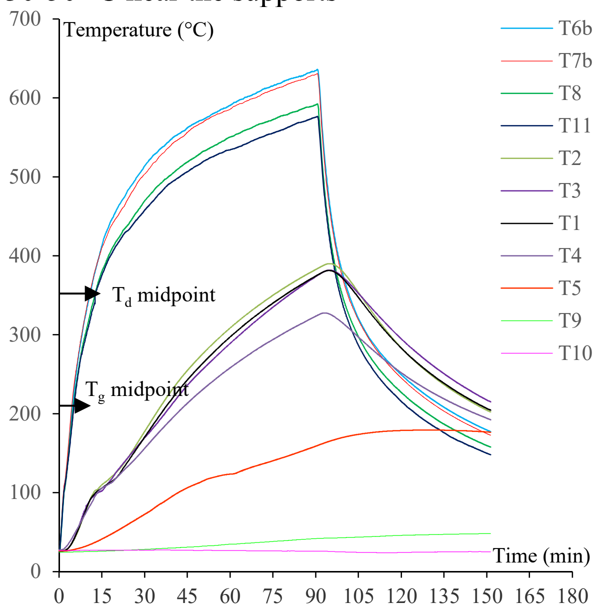

Figure 24. LocH: Temperature versus Time curves

The effectiveness of the strengthening system during a fire event and its residual strength depend on the utilization factor of the member in fire, η_{fi}. The latter is the ratio between the relevant effects of actions in the fire situation at time *t*, $E_{d,fi,t}$, and the design value of the resistance of the member in the fire situation at beginning of thermal transient, $R_{d,fi,0}$ (EN1991-1-2 [25]).

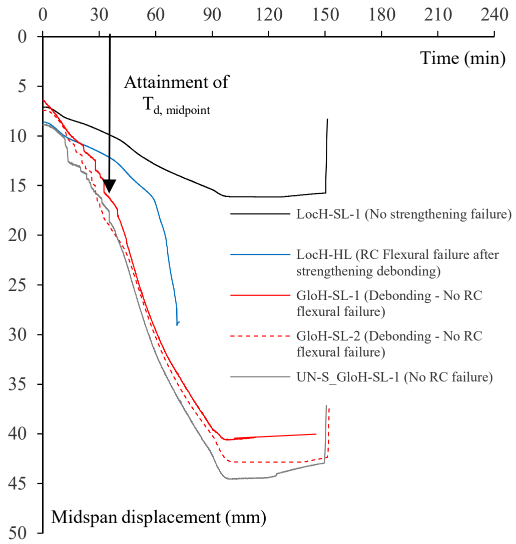

Figure 25 Midspan displacement versus time

GloH-SL

The tests on FRP strengthened beams in the global heating mode were undertaken on beams with a utilization factor equal to about 0.7 (sustained load of 40 kN – GloH-SL). As shown in Figure 25 the beam deflected of about 7 mm, when 40 kN sustained load was attained. Then, when the heating stage started, the deflection increased due to the thermal gradient over the beam, which induced a thermal curvature. It should be noted that, at the attainment of the T_g (max tanδ) in the FRP bar, after about 10 min of heating (25 min by the beginning of the test), no particular changes in the deflection curve were observed. After about 25 min of heating (40 min by the beginning of the test) the FRP bar achieved the decomposition temperature (T_d midpoint - 360°C in Figure 22) along the overall bonded length and a change in the slop of the deflection versus time curve was recorded. This is representative of the transition between the strengthened beam and the un-strengthened one. Moreover, the temperature in the steel rebars, at the same time, attained 100°C, which is the temperature that induces a stiffness reduction. Therefore, the change in displacement slop, observed after about 25 min of heating is also related to the greater deformability of the un-strengthened beam in comparison to that at ambient temperature.

However, the debonding and subsequent loss of effectiveness of the strengthening system did not lead to the failure after 90 min of non-standard heating exposure since the un-strengthened beams were able to carry the applied load without the FRP strengthening system remaining effective, even though very large deflections were exhibited (see Figure 25).

Residual tests, undertaken after the beams had cooled to room temperature, confirmed that the residual failure load was equal to that obtained from testing the un-strengthened beams at ambient temperature (i.e. the pre-existing concrete beams had not been significantly damaged by the heating exposure, despite loss of effectiveness of the FRP system).

LocH-SL

Figure 25 shows that the strengthened beams, tested in local heating configuration with η_{fi} equal to about 0.7– LocH-SL – initially deflected of about 7 mm under the applied load. Then, the midspan deflection increased up to about 16 mm after 90 minutes of non-standard heating exposure, which determined a thermal curvature associated to the thermal gradient over the beam.

The right hand side (RHS) slip was also plotted versus the maximum temperature read by the thermocouples near the midspan (Figure 26), showing that the achievement of the glass transition temperature, first, and of the decomposition temperature, later, did not determine any damage of the strengthening system, since the end-anchorage was still cold. The bar started to slip when its temperature in the midspan achieved about 600°C, whereas the bar was still cold near the supports. It is very likely that a part of the end-anchorage in the unexposed zone, close to the exposed zone, entered in the glass transition stage, reducing the effective end-anchorage length and leading to the slippage of the bar. However, the strengthening system did not fail, as demonstrated via residual tests, since the effective end-anchorage was able to sustain the stress transferred from the midspan when the CFRP in the heated zone completely decomposed. Unfortunately, the effective cold end-anchorage length could not be experimentally determined since no thermocouples were placed on the CFRP bar, in the unexposed zone, in the close vicinity to the exposed zone. However, an estimation of the minimum required effective end-anchorage can be drawn based on the results of bond tests at ambient temperature detailed in Del Prete et al [21] and with reference to the CFRP strain attained in the midspan of the beam, shown in Figure 27. The bond tests showed that, when the bonding length is 300 mm, the failure occurs for debonding at bar/adhesive interface under about 25 kN pull-out load (F_{deb}). The latter determines a strain in the CFRP bar (ε_{deb}) equal to about 3.6‰. Figure 27 shows that the CFRP strain at midspan attained about 3.5‰ during flexural tests. This means that the strengthening system would be effective with a minimum cold end-anchorage length of 300 mm.

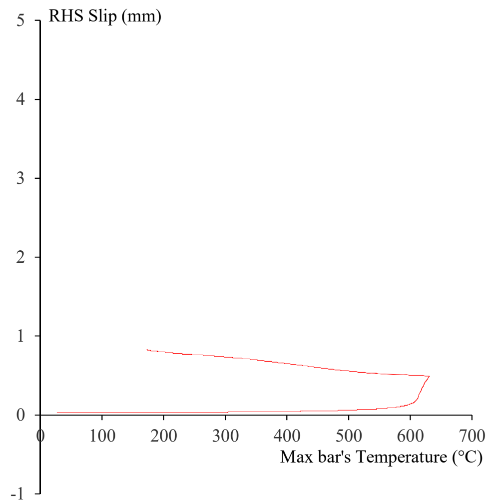

Figure 26 RHS Slip vs Temperature

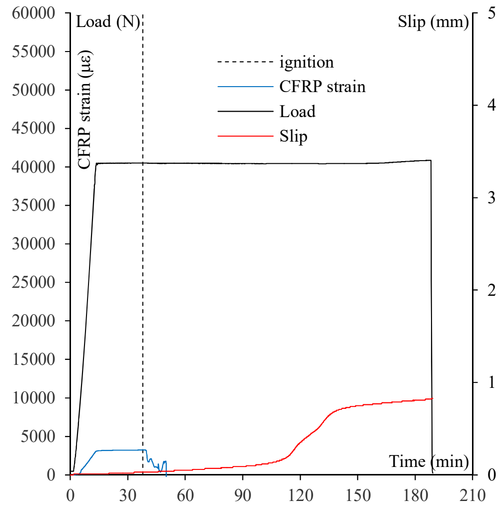

Figure 27 LocH-SL-1. Load, CFRP strain, Slip versus Time

Figure 25 shows also that, in a local heating configuration, the deflection of the beams was significantly lower than that observed in global heating, since the thermal gradient, and therefore the thermal curvature, were lower than those induced by global heating.

LocH-HL

Figure 25 and Figure 28 shows that strengthened beams tested in a local heating configuration with η_{fi} equal to about 0.8 (sustained load of 50 kN) – LocH-HL, were unable to sustain the stress transferred from midspan when the maximum temperature in the CFRP bar ranged between 470÷530°C, even though the temperature near the supports was approximately at ambient.

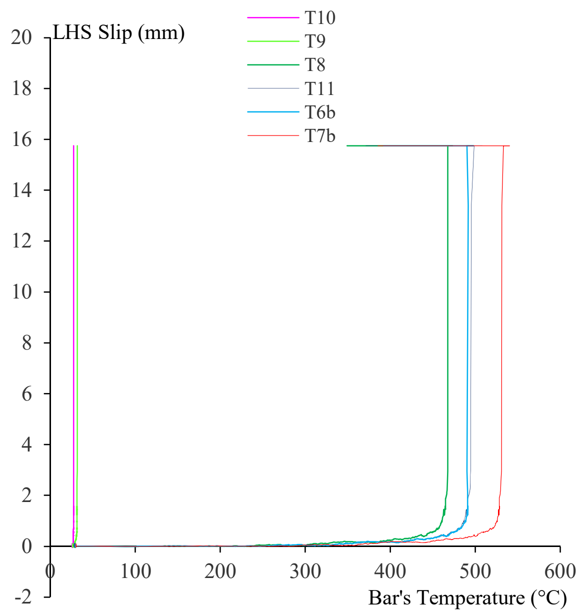

Figure 28 LocH-HL-1. Slip versus Temperature curves

Figure 29a depicts the beam (bottom side) immediately after the failure and proves that the resin of the CFRP bar was completely decomposed in the heated zone, since the temperature at the failure was significantly higher than the decomposition temperature. Conversely, in the unexposed zone, the CFRP bar was not damaged at all. However, it is very likely that the temperature of the CFRP bar close to the heat-exposed zone may have exceeded T_g due to thermal conduction along the FRP bar and this led to a reduction of the effective end-anchorage length.

Figure 29 b depicts the beam (front side) after the failure, showing the distribution of the flexural cracks and the failure mode considered to be a typical post-debonding flexural failure.

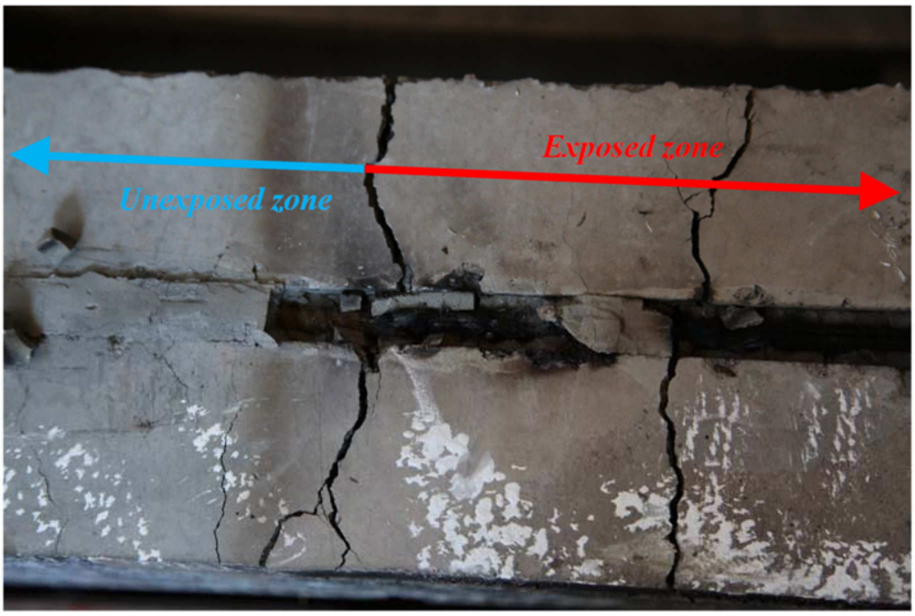

a)

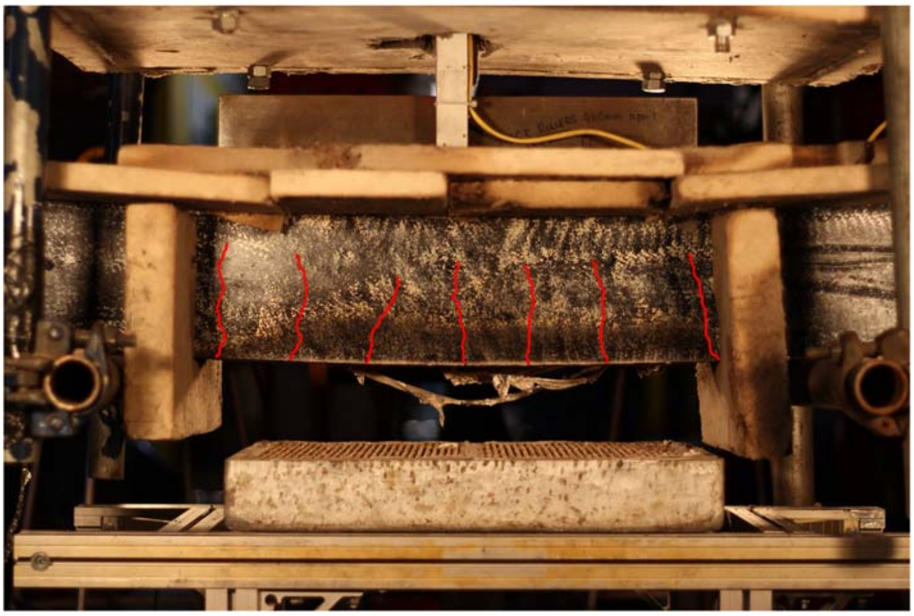

b)

Figure 29 – LocH-HL-1 after failure: a) Bottom side of the beam; b) Front side of the beam

The tests performed herein thus demonstrate the importance of the cold end-anchorage zones to maintain the effectiveness of this NSM FRP strengthening system in case of fire under sustained loads typical of maximum service strain conditions in the FRP. It is noteworthy that no tensile failures of the CFRP bars were observed in any tests, even though (i) a temperature of more than 600°C was attained in the bar during heating, and (ii) a significant sustained stress was maintained within the FRP.

3. PRELIMINARY NUMERICAL SIMULATIONS AND FUTURE WORK

According to European codes, the fire resistance assessment of a structural member may be performed through experimental tests or by applying analytical approaches, whereby conventional temperature-time relationships of the fire environment are usually assumed. For instance, for fires of cellulosic substances, the ISO834 standard curve is suggested by EN1991-1-2. However, standard fire tests have many inadequacies, such as the absence of a cooling phase. Moreover, they do not enable simulation of localised fire events that may occur in real structures. Therefore, the results of non-standard experimental tests, such as those presented herein, cannot easily be used to define a standard time of fire resistance for structural members, since the heating history may be significantly different to that provided by standard fire curves in terms of speed of temperature increasing, maximum temperature, and duration of the heating stage.

Therefore, preliminary numerical analyses, simulating the experimental tests described in this paper, were carried out and presented in detail in Del Prete [26]. Numerical analyses were performed through a relatively simple 2D heat transfer analysis of the cross-sections. The transfer between the rebars and concrete is perfect, as assumed in Del Prete [27], even if Firmo [28] and Bilotta [29] showed that temperature-dependent FRP-concrete interaction should be used when a more in-depth understanding of some local phenomena of stress transfer is necessary.

The aim of these analyses was dual:

1) Assess the ability of simulating the experimental results of non-standard fire tests (local and global heating using propane fired radiant panels);
2) Generalise the experimental results providing a standard time of fire exposure that might lead to the un-effectiveness of the strengthening system due to debonding failure.

The thermal analyses were conducted through the software SAFIR (Franssen [30]). In absence of experimental heating curve measurements, the heat transfer analyses were carried out by imposing on the boundary of the model, the temperature recorded by the thermocouples at the soffit of the beams (Section 2.3.3) during the non-standard tests. The results of the numerical thermal analyses on the 2D cross-sectional and longitudinal finite element models (FEM), shown in Figure 30, were compared with the temperature recorded by the thermocouples during the tests, in order to assess the reliability of the FEM simulating the experimental results.

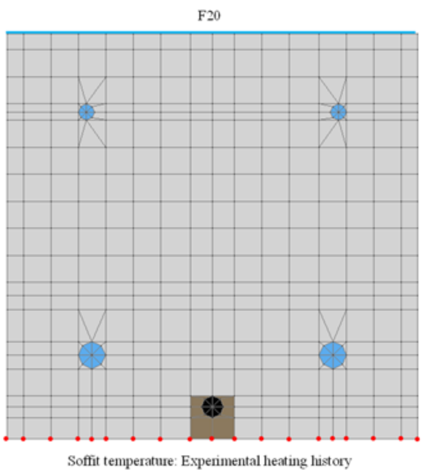

a)

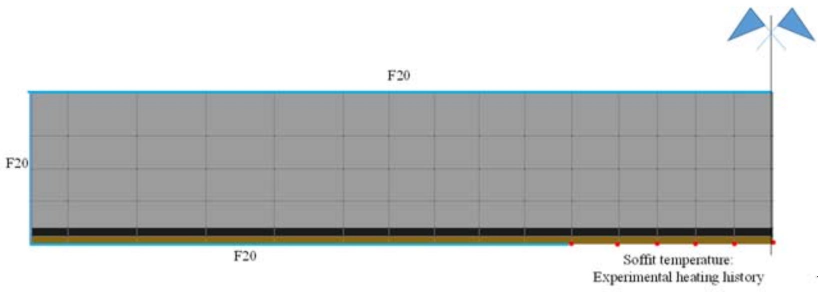

b)

Figure 30 – 2D FEM of NSM FRP strengthened RC beam subjected to the experimental soffit temperature: a) cross-sectional FEM; b) FEM of the longitudinal section

Figure 31 demonstrates that the numerical model is able to predict the temperature and it is a very reliable model, since a good agreement was obtained with the experimental temperatures (thermocouples location is shown in Figure 15). It should be noted that the temperature recorded during the experiments in the unexposed zone in T9 and T10 was about 50°C and 30°C respectively. These temperatures were replicated in the longitudinal heat transfer model, as shown in Figure 31b.

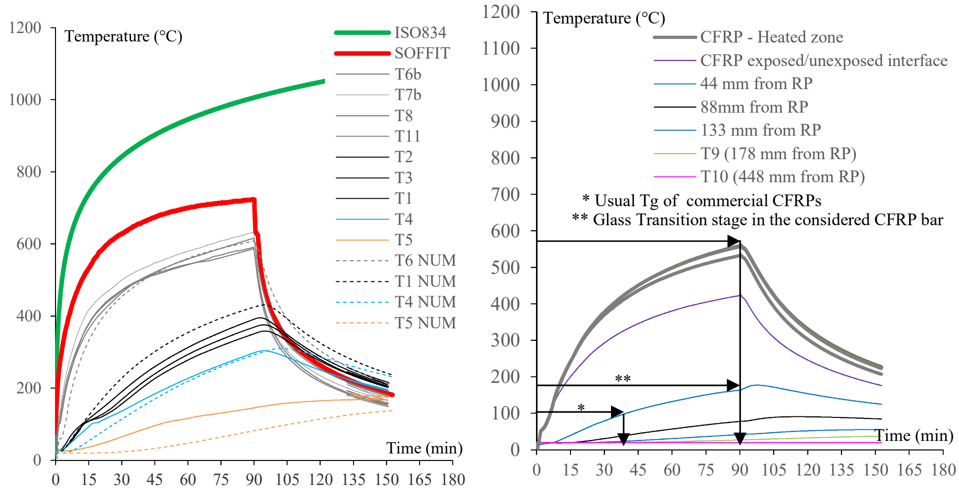

a) b)

Figure 31 – Temperature vs time curves. Numerical-experimental comparison: a) cross-section; b) longitudinal section

The longitudinal thermal model enabled to define the point along the bar entering in the glass transition stage. As shown in Figure 31b, due to the longitudinal thermal conductivity of the CFRP, the model provided a temperature in the bar of about 180°C at 45 mm far from the radiant panel (RP), after about 90 min. This means that the bar, at the interface between the unexposed and exposed zone entered in the glass transition stage.

Once validated the thermal models, the thermal analysis of the cross-sectional FEM, was carried out to define a standard time of ISO834 fire exposure, which may be critical for the effectiveness of the experimentally tested strengthening system. Figure 32 shows that the CFRP bar, after about 15 min of standard fire exposure, achieved 350°C that represents a critical temperature for the effectiveness of the strengthening system in case of global heating, since it leads to the debonding at bar/adhesive interface. Moreover, the numerical thermal model showed that the CFRP bar attained 600°C after about 45 min of standard fire exposure, which may be critical in case of local heating, in case the η_{fi} of the beam is greater than 0.7.

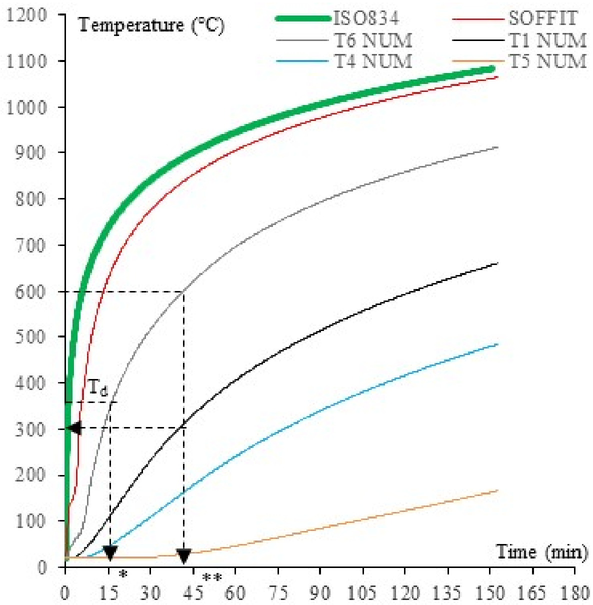

Figure 32 – Temperature vs time curves. Numerical prediction (ISO834) – Experimentally tested strengthening system (*Failure of strengthening in GloH; **Stress transferred to the anchorage in LocH)

However, it should be note that, even if the cold end-anchorage should not be able to sustain the stress transferred from the midspan leading to the loss of strengthening system, the un-strengthened RC beam should be able to sustain a load compatible with its strength at ambient temperature. This is because the temperature in the steel rebars is about 300°C, when the maximum temperature in the CFRP bar is 600°C. Therefore, no strength reduction occurs in RC beam during the fire exposure.

In the frame of future work, tests with an epoxy adhesive rather than the used commercial grout should be carried out before the novel system can be confidently stated as being vastly superior to epoxy-adhered NSM systems.

4. CONCLUSIONS

The available literature about the behaviour of cementitious-bonded Near Surface Mounted (NSM) FRP strengthening systems both at ambient and elevated temperature is very limited, probably due to a presumption that cementitious adhesives are likely to be less effective at room temperature. Therefore, this paper has presented the results of an experimental testing programme to investigate the performance at elevated temperature of a specific novel cementitious-bonded CFRP NSM strengthening system for concrete beams in bending.

Based on the testing presented in this paper, the following key conclusions can be drawn for this system:

- T_g ranged between 160°C ($T_{g,offset}$) and 220°C ($T_{g,max\,(tan\delta)}$) for the CFRP bar used. T_d ranged between 320°C ($T_{d,offset}$) and 360°C ($T_{d,midpoint}$). This highlights the need to standardize T_g and T_d definitions and test configurations.
- The flexural tests of strengthened beams at ambient temperature highlighted that the strengthening provided a considerable increase of the load bearing capacity, with a gain in yielding load ranging between 32-36% and a gain in failure load ranging between 17-25%.
- The capacity of the NSM FRP system depends on the presence of effective cold anchorage, because carbon fibres behave significant strength at elevated temperatures even when the performance of the polymer matrix is compromised;

- When adequately anchored in cool regions with an anchorage length of at least 300 mm, the NSM FRP system studied herein was able to carry tensile stresses typical of in-service conditions at elevated temperatures up to 600°C.
- Local insulation systems placed at the end-anchorages only, instead of insulation the FRP system along the overall bonded length, may be able to prolong the overall system performance in fire; further testing would be required to confirm this.

To generalize the experimental results obtained through the non-standard fire tests and to provide a reliable time of standard fire exposure that may be critical for the NSM FRP strengthened RC beams, thermal numerical analysis of a two-dimensional (2D) cross-sectional finite element model (FEM) of the NSM FRP strengthened RC beam were performed. The input from the beam's soffit temperature, as recorded during the localised heating tests, was used to assess the reliability of the FEM simulating the experimental results. The input from the ISO834 curve was used to define a standard time of fire exposure, which may be critical for the effectiveness of the strengthening both in cases of local and global heating.

Based on the results obtained by the authors and other researchers in the last years by using FEM models for numerical simulation of concrete structures - reinforced or strengthened with FRP - more refined 3D analyses should be performed for a more in-depth understanding of some local phenomena of stress transfer of NSM-FRP systems.

ACKNOWLEDGEMENT

The authors would like to thank Milliken Infrastructure Solutions for providing the FRP materials and cementitious mortar (marketed under the trade name FireStrong) used in the experimental program.

DATA AVAILABILITY

The raw/processed data required to reproduce these findings cannot be shared at this time due to technical or time limitations

REFERENCES

1. El-Hacha R., Rizkalla S: H., (2004). Near-Surface-Mounted Fiber-Reinforced Polymer Reinforcements for Flexural Strengthening of Concrete Structures, ACI Structural Journal, September-October 2004, 717-726
2. Foret G., Limam O., (2008). Experimental and Numerical analysis of RC two-way slabs strengthened with NSM CFRP rods, Construction and Building Materials 22 (2008) 2025-2030
3. Bilotta A., Ceroni F., Di Ludovico M., Nigro E., Pecce M., (2011). Bond Efficiency of EBR and NSM FRP Systems for Strengthening Concrete Members, J. Compos. Constr. 2011.15:757-772
4. Yu B., Kodur V., (2014). Fire behavior of concrete T-beams strengthened with near-surface mounted FRP reinforcement. Engineering Structures. 2014;80:350-361.
5. Petri P., Blaszak G., Rizkalla S., (2013). Structural Fire Endurance of an RC Slab Strengthened with High T_g Near Surface Mounted CFRP Bars. ACIC 2013, Edited by Miss Claire. J. Whysall and Prof. Su. E. Taylor, 140-151, Queen's University Belfast on 10 -12 September 2013

6. Burke P.J., Bisby L. A., Green M., (2013). Effects of elevated temperature on near surface mounted and externally bonded FRP strengthening systems for concrete. Cement & Concrete Composites 35 (2013) 190–199
7. Palmieri A., Matthys S., Taerwe L., (2013). Fire Endurance and Residual Strength of Insulated Concrete Beams Strengthened with Near-Surface Mounted Reinforcement. J. Compos. Constr. 2013.17:454-462
8. Blontrock H., Taerwe L., Vandevelde, P. (2001) Fire Testing of Concrete Slabs Strengthened with Fibre Composite Laminates, The Fifth Annual Symposium on Fibre-Reinforced-Plastic Reinforcement for Concrete Structures (FRPRCS-5). Edited by C. Burgoyne, Thomas Telford, London, 547-556
9. Bisby L.A., Green M.F., Kodur V.K.R (2005a). Response to fire of concrete structures that incorporate FRP, Prog. Struct. Engng. Mater., 7:136-149
10. Williams B., Kodur V., Green M., Bisby L., (2008). Fire endurance of Fiber-Reinforced Polymer Strengthened Concrete T-Beams ACI Structural Journal, 105(1), 60-67
11. Palmieri, A., Matthys S., Taerwe L., (2010). Experimental Investigation on bond of NSM strengthened RC structures, proceeding CICE 2010, September 27-29, 2010 Beijing, China
12. Palmieri A., Matthys S., Taerwe L. (2010). Strengthening with Near Surface Mounted Reinforcement: Structural and Fire behavior, 3rd fib 2010 Washington DC,USA
13. Firmo J. P., Correia J. R., França P., (2012). Fire behaviour of reinforced concrete beams strengthened with CFRP laminates: Protection systems with insulation of the anchorage zones, Composites: Part B 43 (2012) 1545–1556
14. Palmieri, A., Matthys S., Taerwe L., (2011a). Fire testing of RC beams strengthened with NSM reinforcement, 10th International Symposium Fiber-Reinforced Polymer Reinforcement for Concrete Structures, Editors: Rajan Sen, Rudolf Seracino, Carol Shield, Will Gold, 51_1-51_16, 2-4 April 2011, Tampa, Florida (USA)
15. Palmieri A., Matthys S., Taerwe L., (2013). Fire Endurance and Residual Strength of Insulated Concrete Beams Strengthened with Near-Surface Mounted Reinforcement, J. Compos. Constr. 2013.17:454-462
16. Kodur V. K. R., Yu B., (2013). Evaluating the Fire Response of Concrete Beams Strengthened with Near-Surface-Mounted FRP Reinforcement, J. Compos. Constr. 2013.17:517-529
17. FireStrong™ Grout Pumpable Grout, Technical Data Sheet, March 2014.
18. ISO 6721-1:2011. Plastics - Determination of dynamic mechanical properties - Part 1: General principles
19. DIN 65 583 (1999). "Aerospace - Fibre reinforced materials - Determination of glass transition of fibre composites under dynamic load
20. Griffis, C.A., Masmura, R.A., & Chang, C.I. 1(984). Thermal response of graphite epoxy composite subjected to rapid heating. In Environmental Effects on Composite Materials, Vol. 2, Technomic Publishing Company, Lancaster, Pennsylvania, 245-260.
21. Del Prete I., Bilotta A., Bisby L., Nigro E., (2018). Ambient temperature performance of cementitious matrices for fire-safe NSM FRP strengthening of concrete structures, Construction and Building Materials 193 (2018) 42–54
22. ASTM D 4092 – 07 (2013). Standard Terminology for Plastics: Dynamic Mechanical Properties
23. EN1992-1-1 (2004). Eurocode 2: Design of concrete structures - Part 1-1: General rules and rules for buildings
24. ACI 318-08 (2009). Building Code Requirements for Structural Concrete. ACI Committee 318, American Concrete Institute
25. EN1991-1-2 (2002). Eurocode 1: Actions on structures – Part 1-2: General actions – Actions on structures exposed to fire

26. Del Prete I., (2015). NSM FRP strengthening RC beams using high Tg FRPs & cementitious adhesives – Response at Ambient and Elevated temperature. PhD Thesis. http://www.fedoa.unina.it/10475/1/DelPrete_Iolanda_XXVII.pdf
27. Del Prete I., Bilotta A., Nigro E. (2015) Performances at high temperature of RC bridge decks strengthened with EBR-FRP. Composites Part B: Engineering 68, 27-37. https://doi.org/10.1016/j.compositesb.2014.08.011
28. Firmo J.P., Arruda M.R.T., Correia J.R., Rosa I.C. (2018). Three-dimensional finite element modelling of the fire behaviour of insulated RC beams strengthened with EBR and NSM CFRP strips. Composite Structures Volume 183, 1 January 2018, Pages 124-136. https://doi.org/10.1016/j.compstruct.2017.01.082
29. Bilotta A., Compagnone A., Esposito L., Nigro E. (2020) Structural behaviour of FRP reinforced concrete slabs in fire. Engineering Structures. Volume 221, 15 October 2020. https://doi.org/10.1016/j.engstruct.2020.111058
30. Franssen, J-M. 2005. "SAFIR: A thermal/structural program for modelling structures under fire." Engineering Journal-American Institute of Steel Construction Inc pp. 143-158.